Coexistence of in-plane and out-of-plane remanences of metastable body-centered-cubic Co islands in Au matrix

T. Miyamachi,[1,*] T. Kawagoe,[2] S. Imada,[1] M. Tsunekawa,[1] H. Fujiwara,[1] M. Geshi,[1] A. Sekiyama,[1] F. H. Chang,[3] H. J. Lin,[3] C. T. Chen,[3] F. Kronast,[4] H. Dürr,[4] K. Fukumoto,[5] and S. Suga[1]

[1]*Graduate School of Engineering Science, Osaka University, Toyonaka, Osaka 560-8531, Japan*
[2]*Division of Natural Science, Osaka Kyoiku University, Kashiwara, Osaka 582-8582, Japan*
[3]*National Synchrotron Radiation Research Center, 101 Hsin-Ann Road, Hsinchu 30076, Taiwan*
[4]*Helmholtz Zentrum Berlin für Materialien und Energie, BESSY II, Albert-Einstein-straße 15 Berlin 12489, Germany*
[5]*Japan Synchrotron Radiation Research Institute, Mikazuki, Sayo, Hyogo 679-5198, Japan*

(Dated: February 14, 2012)

We studied the relationship between magnetism and morphology of metastable bcc Co nanostructures on Au(001) by x-ray absorption magnetic circular dichroism in combination with scanning tunneling microscopy and photoelectron emission microscopy. While room temperature deposition of Co onto Au(001) leads to the formation of bcc Co thin films with pure in-plane magnetization, post-annealing of these thin films at 500 K drastically changes the morphology to bcc Co islands embedded in Au. In accordance with this morphological change, we find that an out-of-plane magnetization appears and in-plane and out-of-plane remanent magnetizations coexist in the islands. The nanostructure-size dependence of magnetic moments discloses the dominant role of rim atoms for the out-of-plane magnetization and core atoms for the in-plane magnetization. Within the proposed rim-core model, the origin of this complex noncollinear magnetic structure could be ascribed to the giant magnetic anisotropy and the spin rotation of rim atoms.

PACS numbers: 75.50.-y, 75.70.-i, 68.37.-d

I. INTRODUCTION

The final goal of miniaturization for information storage is to realize extremely small magnetic bits operating at room temperature. For this purpose, tiny bits must overcome thermal fluctuation. The thermal stability of bits relies on a magnetic anisotropy energy (MAE). Recent experimental and theoretical advances in nanoscale magnetic systems have revealed the key concepts to the giant MAE of nanostructures, i.e., (i) lowering the coordination number of atoms[1], (ii) interfacial effect with surroundings[2] and (iii) electronic band structures[3]. So far, (i) was mainly emphasized to enhance the MAE of magnetic atoms. As the atomic coordination is reduced from bulky materials to thin films and further to two-dimensional (2D) nanostructures, the orbital magnetic moment is enhanced, resulting in a giant MAE per atom[1,4] since the MAE and orbital magnetic moment are linked via spin-orbit (SO) interaction[5]. Within 2D nanostructures, larger magnetic moments and MAE of rim atoms owing to the lower symmetry compared to core atoms are also reported[6–8]. On the other hand, the reduction of volume through bulk, thin films and 2D nanostructures leads to weaker ferromagnetic coupling energy in finite-sized 2D nanostructures, inducing the random flipping of the magnetic moment (superparamagnetism[9]) at higher temperatures of practical interest. Until now, room temperature ferromagnetism is reported for three-dimensional (3D) nanoparticles with large MAEs arising from the formation of superlattices[10] or exchange bias[11]. However, the difficulty is to evaluate their morphology on the nanoscopic scale. In addition, random magnetic easy axes of 3D nanoparticles prohibit one from investigating the origins of their MAEs. One possible approach to enhance the MAE of finite-sized 2D nanostructures is to fabricate pseudo 3D nanostructures by vertically stacking atoms while keeping the lateral size. In such nanostructures, the MAE could be enhanced compared to simple 2D nanostructures with the same lateral size due to the increased volume. Despite the merit of vertical stacking, one should remember the technological difficulty to stack a sufficient number of atoms to be ferromagnetic at room temperature. Hence, incorporation of (ii) and (iii) in the vertical stacking is a promising direction toward practical nanostructure fabrication.

To fulfill these conditions, we artificially grow pseudo 3D bcc Co islands embedded in Au in this study. In addition to the vertical stacking, the interfacial effect with surrounding Au atoms and characteristic electronic band structures of metastable bcc Co phase could further enhance the MAE of islands than simple lowering of the atomic coordination, resulting in room temperature ferromagnetism. The experimental results suggest that the observed coexistence of out-of-plane and in-plane remanent magnetizations in islands derives from the rim and core regions, respectively.

II. EXPERIMENTAL DETAILS

A reconstructed Au(001) surface was first grown on a 3 nm-thick Cr precovered MgO(001)[12]. All samples in this study were prepared by molecular beam epitaxy (MBE) from a high-purity Co rod (99.998 %) onto this Au(001)

surface. The base pressure of the MBE chamber was below 5×10^{-11} Torr. Since highly characterized samples are needed to investigate the relationship between magnetism and morphology, their morphology is first accurately determined by scanning tunneling microscopy (STM) in a constant-current mode at room temperature. Then 2nm Au is evaporated on samples *in situ* before transportation through the atmosphere to chambers for magnetic measurements. Such capping prevents oxidation in atmospheric conditions while allowing the detection of magnetic signals.

Magnetic moments of samples were investigated by x-ray magnetic circular dichroism (XMCD). The measurements were performed at Dragon beamline BL11A of NSRRC in Taiwan by the total-electron-yield method at room temperature. The energy resolution $E/\Delta E$ was better than 10, 000 and the circular polarization of the incident x-ray was 83 %. In the XMCD measurements, the circular polarization of the x-ray was fixed and the direction of the applied magnetic field up to 1 T was reversed. The magnetization directions of magnetic domains at remanence are determined by photoelectron emission microscope combined with XMCD (XMCD-PEEM) at room temperature. Measurements were performed at UE49-PGMa of BESSY in Germany. The incident circular x-ray was nearly full polarized. XMCD and XMCD-PEEM measurements were reproduced at BL25SU[13] of SPring-8 in Japan.

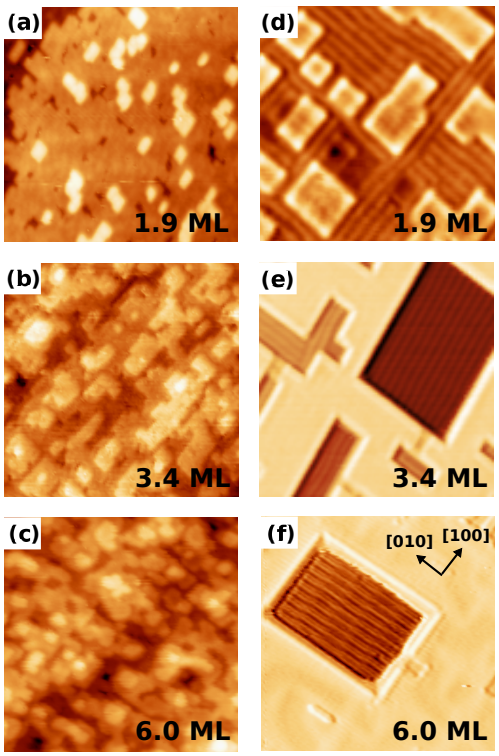

FIG. 1: (Color online) STM images of (a) 1.9 ML, (b) 3.4 ML, (c) 6.0 ML bcc Co thin films (RT) and (d) 1.9 ML, (e) 3.4 ML, (f) 6.0 ML bcc Co nanostructures (PA) on Au(001). The size of each image is 24 × 24 nm^2.

III. RESULTS AND DISCUSSION

A. Morphology

To prepare bcc Co nanostructures, we first grow bcc Co thin films by room temperature deposition of Co onto Au(001) (these samples are hereafter called RT). Figure 1(a) shows the STM image of 1.9 monolayer (ML) Co on Au(001) grown at room temperature (hereafter expressed as 1.9 ML RT). Its morphology is composed of the film surface with small islands. From the characteristic 1 ML height difference of about 0.14 nm and p(1×1) low energy electron diffraction (LEED) pattern with a lattice constant of about 0.28 nm, it is found that deposited Co is epitaxally grown on Au(001) with bcc phase[14]. As the coverage is increased up to 3.4 and 6.0 ML as shown in Figs. 1(b) and 1(c), the island growth is promoted, resulting in rough surfaces. However, we also confirm from height profiles and LEED patterns that the bcc structure is still maintained at these coverages.

Pseudo 3D bcc Co nanostructures are fabricated by post-annealing of bcc Co thin films (RT) at 500 K (these samples are hereafter called PA). The surface of PA prepared from 1.9 ML RT (expressed as 1.9 ML PA) is composed of the reconstructed Au(001) surface and rectangular islands as shown in Fig. 1(d). Gaussian fitting of the size distribution of 363 islands in the whole measured region in Fig. 2(a) leads to a mean lateral dimension of 3.8 nm with FWHM of 1.8 nm. The morphology of islands was determined by STM to be 4 (5) ML bcc Co with 2 (1) ML Au surfactant layer in the rim (core) region as shown in Fig. 2(b) (details are given in ref.12). The rim width of about 0.5 nm corresponds to four atoms numbered as 1 - 4. The slight difference of height between the rim and core regions (0.06 nm) shown in Fig. 2(c) is caused by 1 ML height difference between Au(001) and bcc Co (001) [Au: 0.20 nm, bcc Co: 0.14 nm]. The origin of pseudo 3D bcc Co islands embedded in Au would be due to the immiscibility of these two metals and large difference in their surface free energies[15]. In this study, three nanostructures with different morphology were prepared by changing Co coverage. The morphology changes from isolated islands in 1.9 ML PA to network structures in 3.4 ML PA (Fig. 1(e)) due to the coalescence of islands. In 6.0 ML PA, the coalescence is further promoted, resulting in a considerably reduced fraction of the rim (Fig. 1(f)).

B. Magnetic moments I

The magnetism of PA is studied and compared to that of RT by using XMCD. XMCD spectra are obtained in the total-electron-yield mode at room temperature by detecting I_+ - I_-, where I_+ and I_- denote the x-ray absorp-

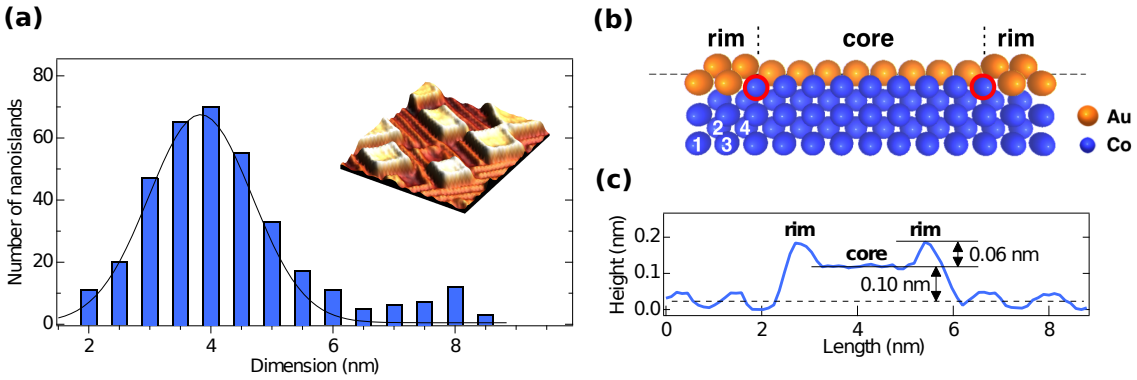

FIG. 2: (Color online) (a) Size distribution of bcc Co islands. Lateral dimension is given by substituting each island by a square with the same area. (b) Schematic cross-sectional view of a bcc Co island. Orange and blue spheres represent Au and Co atoms. Numbers show the column number of Co atom in the rim. Outside the rim, Au atoms are piled up to the level shown by the dashed horizontal line. (c) Height profile of a typical bcc Co island (1.9 ML PA). The dashed horizontal line is set to zero.

tion spectra (XAS) with the photon spin parallel and antiparallel to the magnetic field $\mathbf{B}$ of 1T. $\mathbf{B}$ was applied either parallel to the sample surface ($\mathbf{B}_{\parallel}$) or perpendicular to it ($\mathbf{B}_{\perp}$). The photon incidence angle is deviated by 30° from the direction of $\mathbf{B}$. For the XMCD measurement, the direction of $\mathbf{B}$ is reversed. Then, the spectra for $\mathbf{B}_{\parallel}$ and $\mathbf{B}_{\perp}$ are sensitive to the in-plane and out-of-plane magnetizations of samples. Figure 3(a) shows XAS and XMCD spectra of 3.4 ML RT at the Co $L_{2,3}$ absorption edges. An XMCD signal is only observed for the $\mathbf{B}_{\parallel}$. The absence of the out-of-plane magnetization and a strong in-plane XMCD are consistent with previous results[16], reflecting the strong in-plane uniaxial anisotropy of bcc Co thin films[17,18]. The in-plane magnetization might show up in the XMCD spectrum recorded in the $\mathbf{B}_{\perp}$ geometry in our XMCD alignment. Nevertheless, note that the $\mathbf{B}_{\perp}$ XMCD signal is neither seen for 1.9 and 6.0 ML RT. This is because the in-plane magnetization of all the sample is averaged out by demagnetization before $\mathbf{B}_{\perp}$ XMCD measurements. Hence, we emphasize in this study that the out-of-plane magnetization and the in-plane magnetization are disentangled in the $\mathbf{B}_{\perp}$ geometry, and any $\mathbf{B}_{\perp}$ XMCD signals are only attributable to the out-of-plane magnetization of the sample.

If PA has similar magnetic properties as RT, no $\mathbf{B}_{\perp}$ XMCD is expected. However, in addition to the in-plane magnetization, 3.4 ML PA shows the out-of-plane magnetization (Fig. 3(b)). Comparing the XMCD spectrum of 3.4 ML RT with that of 3.4 ML PA, it is obvious that nanostructuring (PA) of the thin film induces the out-of-plane magnetization. Figure 4(a) displays a series of XMCD spectra of PAs as a function of Co coverage recorded in the $\mathbf{B}_{\perp}$ geometry. The out-of-plane magnetization is clearly observed in all PAs. Furthermore, it turns out that the magnitude of XMCD at the L_3 edge relative to the L_2 edge increases systematically with decreasing Co coverage. An even more intriguing feature of PA is seen in the remanent magnetization. We have confirmed from the remanent $\mathbf{B}_{\perp}$ XMCD and longitudinal Kerr signals in Figs. 4(b) and 4(c) that 1.9 ML PA is ferromagnetic at room temperature and shows both (b) out-of-plane and (c) in-plane remanences. As for the origin of remanences, coalescences or interactions between islands are not probable. This is because reduced remanent $\mathbf{B}_{\perp}$ XMCD signal with increasing Co coverage is observed (not shown here), in contrast to the coalescence-induced ferromagnetism of Co/Au(111) system[19]. In addition, the average distance between adjacent Co islands here is comparable to or greater than that of non-interacting Co islands on Au(788)[20]. Hence, these results provide a clear evidence of coexisting out-of-plane and in-plane remanences within the island.

To elucidate the origin of coexisting remanences, the morphological dependence of out-of-plane orbital ($L_{\perp}$) and spin ($S_{\perp}$) magnetic moments observed only in PAs is examined by XMCD sum rules[21,22]. It should be noted, however, that evaluated magnetic moments of PAs are lower limits since the highest available field of $\mathbf{B}_{\perp} = 1$ T may not be enough to confirm full saturation of PA samples. The number of 2.22 Co 3d holes, obtained from our *ab initio* calculation, is used here. We find that $L_{\perp}$ increases with decreasing Co coverage as shown by red squares in Fig. 5(a) (0.03 ± 0.01, 0.11 ± 0.01 and 0.14 ± 0.02 μ_B/atom for 6.0, 3.4 and 1.9 ML PA, respectively). This $L_{\perp}$ behavior is seen in other systems and is related to the increased fraction of low coordinated atoms in the nanostructure[1,6]. Nanostructuring could enhance not only L but also S[4]. However, $S_{\perp}$ of PAs, 0.10, 0.33 and 0.42 μ_B/atom for 6.0, 3.4 and 1.9 ML PA, respectively, shown by red squares in Fig. 5(b) is even smaller than the in-plane spin magnetic moment $S_{\parallel}$ of thick bcc Co films (1.44 μ_B/atom[16]).

C. Magnetic structure

To interpret such unexpectedly small $S_{\perp}$, we consider genuine magnetic structures of PA based on the atomic

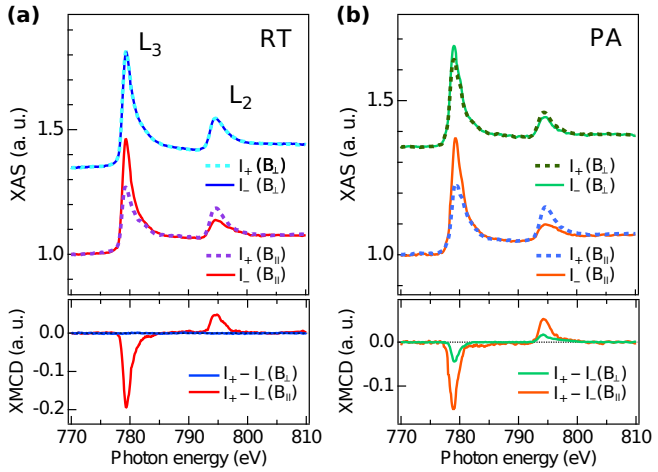

FIG. 3: (Color online) $L_{2,3}$ XAS and XMCD spectra of 3.4 ML (a) bcc Co thin film (RT) and (b) bcc Co nanostructures (PA) with respect to the external magnetic field $\mathbf{B}$ of 1 T measured in the $\mathbf{B}_\perp$ and the $\mathbf{B}_\parallel$ geometries. The XAS spectra are normalized by the pre-edge intensity at 770 eV.

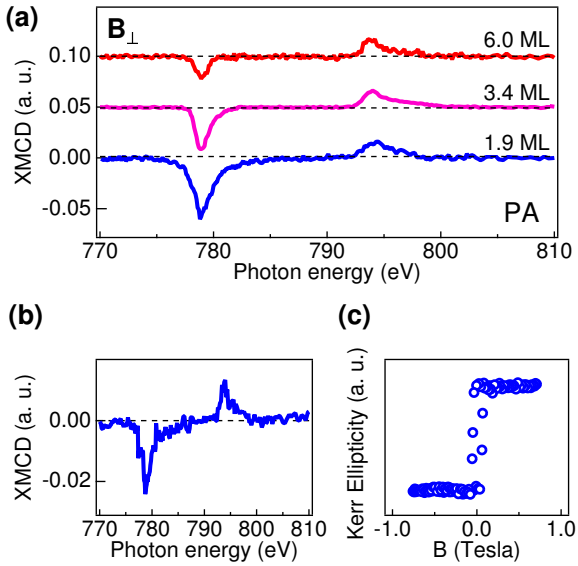

FIG. 4: (Color online) (a) XMCD spectra of bcc Co nanostructures (PA) as a function of Co coverage measured in the $\mathbf{B}_\perp$ geometry. The spectra are normalized to the L_2 intensity. (b) The out-of-plane remanent XMCD spectrum of 1.9 ML PA measured in the $\mathbf{B}_\perp$ geometry. (c) The in-plane easy axis hysteresis loop of 1.9 ML PA obtained by longitudinal Kerr effects measured at room temperature. The magnetic field is applied along [110] direction of bcc Co.

coordination. The morphological dependence of $L_\perp$ in PAs and the absence of $L_\perp$ and $S_\perp$ in RTs (blue triangles in Fig. 5) suggest first that the atomic sites with reduced coordination existing only in PAs give rise to the out-of-plane magnetization. Obviously, the rim atoms satisfy these conditions. Secondly, one can expect a distinct difference in magnetic properties between the rim and core atoms in PAs due to the different atomic coordination. Namely, the core atoms are magnetized in-plane and their $L_\perp$ and $S_\perp$ are zero because of the similar atomic coordination as in RTs[23]. For such nanostructures, coexisting remanences are expected, and $L_\perp$ and $S_\perp$ obtained by XMCD can be underestimated since XMCD provides the average magnetic moments.

Besides the proposed rim-core model magnetic structure, the low out-of-plane magnetization could also appear in the XMCD in the following cases; (1) partial rotation of Co moments caused by the external $\mathbf{B}_\perp$ field in such a case as the easy axis is toward in-plane directions, or (2) a particle dependence, i.e., some islands favor the out-of-plane magnetization, while others are likely to be magnetized in-plane, or (3) a canted easy axis of magnetization. In the case (3), the magnetization direction of whole nanostructures deviates from pure in-plane or out-of-plane directions and hence both $\mathbf{B}_\perp$ and $\mathbf{B}_\parallel$ XMCD signals could also be detected.

However, these possibilities can be excluded as follows. As for (1), the behaviors of $L_\perp$ and $S_\perp$ are inconsistent with the partial rotation. Such external-field-induced magnetization would be larger with increasing Co coverage since smaller MAE is expected according to the quenching of the orbital moment due to stronger crystal field. This possibility is, however, definitely ruled out by our experimental results. In addition, the out-of-plane remanence should not be observed in this case, in contrast to our observation (Fig. 4(b)).

As for (2), such a 90° shift of the magnetization direction, which is a kind of a spin reorientation transition (SRT), could be closely related to the thickness and strains near the interface or surface of nanostructures[24]. The thickness of capping layer is also an important factor to induce the SRT[25]. However, these factors are identical for islands in this study and hence the SRT among islands is not probable. In our knowledge, the difference in the lateral size leads to the different magnitude of magnetic moments due to the localization or delocalization of the electronic states near the Fermi energy[1], and not to the difference in the magnetization direction. Furthermore, this possibility cannot explain lower magnetic moments at higher coverages since the islands are just coalesced.

As for (3), the easy magnetization direction of nanostructures is determined by the competition between the symmetry of crystal structure (magnetocrystalline magnetic anisotropy) and morphology (shape magnetic anisotropy), and is normally toward pure in-plane or out-of-plane directions at the remanence[9]. When nanostructures are supported by surfaces or capped, the situation might totally change due to interfacial-strain-induced atomic relaxation, which could lead to the modification of the easy axis of magnetization and MAE of nanostructures. Indeed, Nahas et al. demonstrated that the MAEs of Co nanodots on Au(111) changed drastically during Au encapsulation[26]. This is due to the change

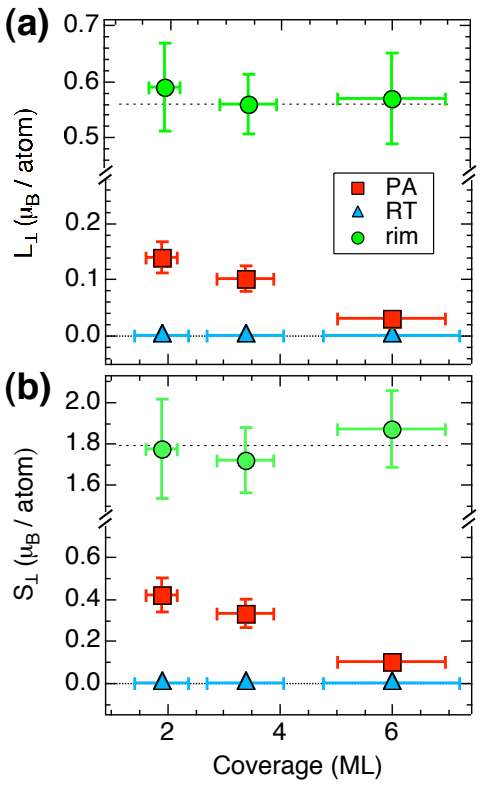

FIG. 5: (Color online) Out-of-plane orbital and spin magnetic moments, (a) $L_\perp$ and (b) $S_\perp$, of bcc Co nanostructures (PA: red squares) and thin films (RT: blue triangles) as a function of Co coverage. The horizontal error bars represent the deviations of the coverage determined by STM and the quartz crystal oscillator. The standard deviations of the estimated magnetic moments are shown by the vertical error bars. The values of the orbital (spin) magnetic moment of the rim atoms, $L_\perp^{rim}$ ($S_\perp^{rim}$): green circles, are obtained by $L_\perp/f_{rim}$ ($S_\perp/f_{rim}$) for each coverage. The dashed lines are guides to eyes, showing the constant $L_\perp^{rim}$ and $S_\perp^{rim}$ with respect to the Co coverage.

of atomic lattice parameters of the whole Co nanodots caused by the large lattice mismatch between Au(111) and hcp Co(111) ($\sim$ 14 %[27]). However, in the present study, the lattice mismatch between Au(001) including Au cap and bcc Co(001) is only $\sim$ 1.7 %[12,14] and hence the atomic relaxation is negligible in both RT and PA. In case the atomic relaxation is active, the MAE should change at least in a thin film with the coverage of 1.9 ML, where the influence from Au substrate and Au cap is significant. The absence of the $\mathbf{B}_\perp$ XMCD signal of 1.9 ML RT is in contrast to this expectation. The canted easy axis can be also excluded by the XMCD-PEEM as explained in detail in the next paragraph.

Eventually, we consider that the proposed rim-core model is the most probable magnetic structure of PA. It should be noted that this complex magnetic structure is also proposed in other systems[6–8]. Direct evidence of the rim-core magnetic structure may be provided with spin-polarized STM. However, this technique is not proper in this study due to the presence of the Au surfactant layer. Instead, we have performed magnetic imaging with element specific XMCD-PEEM to confirm intrinsic in-plane magnetization of the core atoms. With this technique, we can separately extract the magnetic information of bcc Co nanostructures from the Au surfactant layer and Au cap. In XMCD-PEEM, the remnant magnetization directions of domains are distinguishable from the azimuthal angular (Φ) dependence of the magnetization $\mathbf{M}$ while imaging domains as shown in Fig. 6(a). Since the XMCD intensity of magnetic domains is proportional to the projection of the magnetic moment $\mathbf{M}$ toward the direction of the incident x-ray in XMCD-PEEM, a cosine (or sine) behavior as a function of Φ is expected for the in-plane magnetization (pink arrows) and constant behavior is expected for the out-of-plane magnetization (green arrows). In case of canted magnetization, $\mathbf{M}$ follows a cosine (or sine) behavior but does not show zero at the minimum.

Figure 6(b) shows an XMCD-PEEM image of 6.0 ML PA, which is suitable to investigate the magnetic properties of the core atoms. With increasing coverage (or the lateral size of nanostructures), multi-domain structures are formed. However, the easy axes (in-plane or out-of-plane) of each domain could be identical to those of a single domain due to the same thickness as mentioned above. Hence, obtained results could be also applicable to PAs with lower coverages. Figure 6(c) shows the Φ dependence of $\mathbf{M}$ for white contrast domains in the XMCD-PEEM image. The [110] direction is defined as $\Phi = 0°$. $\mathbf{M}$ follows a cosine behavior with a positive maximum at 0° and zero at 90°, representing the magnetization direction along [110] (red arrow), which excludes the possibility of canted magnetization of bcc Co nanostructures. In the same way, magnetization directions of all the other domains are also found to be toward in-plane <110> directions (green and blue arrows), likewise the case of 1.9 ML PA (Fig. 4(c)), validating that the core atoms are in-plane magnetized and their easy magnetization directions are independent of Co coverage. The evaluated in-plane orbital magnetic moment of the core atoms ($L_\parallel^{core}$) of white contrast domains at $\Phi = 0°$, 0.27 $\pm$ 0.02 μ_B/atom, is in good agreement with $L_\parallel$ of 3.4 ML RT, 0.28 $\pm$ 0.04 μ_B/atom, derived from the XAS and XMCD spectra shown in Fig. 3(a). Comparable values of $L_\parallel^{core}$ of PA and $L_\parallel$ of RT further ensure the similar magnetic properties of the core atoms in PA as those of RT.

Interestingly, we observed only in-plane magnetization and no out-of-plane magnetization. This is well understood by considering the rim-core magnetic structure since a spatial resolution of 20 nm in the present XMCD-PEEM measurements is not enough to detect the out-of-plane magnetization signals resulting from the rim atoms.

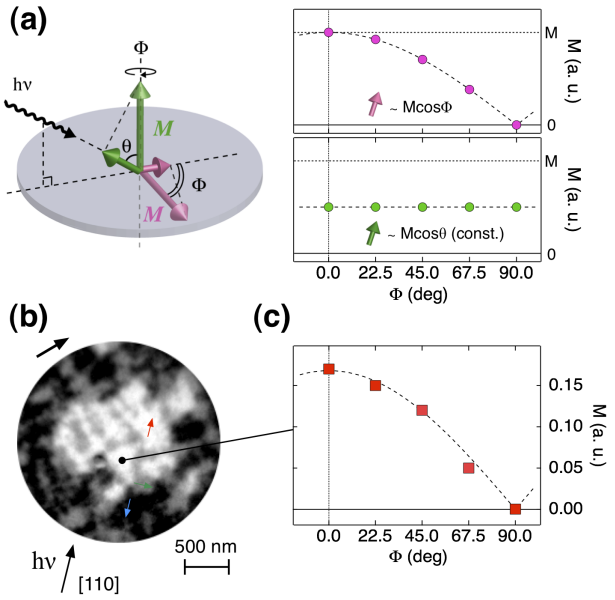

FIG. 6: (Color online) (a) Schematic explanation of the azimuthal angular (Φ) dependence of the magnetization **M**. For in-plane magnetization, the projection of **M** follows a cosine function (McosΦ) as shown by pink arrows. For out-of-plane magnetization, the projection is independent of Φ, providing a constant value (Mcosθ) as shown by green arrows, where θ is the polar angle between the surface normal and the incident x-ray. In this study, θ is set to 60°. (b) XMCD-PEEM domain image of 6.0 ML bcc Co nanostructure (PA), obtained by tuning the photon energy to the maximum of the Co L_3 absorption edge (∼ 778 eV). The direction of hν is parallel to [110] of bcc Co at Φ = 0°. Local magnetization directions are shown by red, green and blue arrows inside each domain. (c) The Φ dependence of **M** for white contrast domains. **M** is obtained by the intensity of the L_3 edge XMCD peak (∼ 778 eV) of the domains as a function of Φ. Each point is normalized by the pre-edge intensity at 775 eV. The sample is rotated from Φ = 0° to 90° in steps of 22.5° in a clockwise direction.

D. Magnetic moments II

Room temperature out-of-plane remanence caused by a small amount of the rim atoms suggests their large out-of-plane magnetic moments. The magnetic moments of the rim atoms can be extracted through the following equation of magnetic moments obtained by XMCD on the rim-core model. Namely, $M_\perp^{rim} f_{rim} + M_\perp^{core}(1 - f_{rim}) = M_\perp$ (M = L, S), where $M_\perp^{rim}$ ($M_\perp^{core}$), $M_\perp$ and f_{rim} denote the magnetic moments of the rim (core) atoms, average magnetic moments and fraction of the rim atoms giving rise to the out-of-plane magnetization. Considering $L_\perp^{core}$ ($S_\perp^{core}$) ∼ 0 as manifested above, $L_\perp^{rim}$ ($S_\perp^{rim}$) is given by $L_\perp/f_{rim}$ ($S_\perp/f_{rim}$). By virtue of STM, we can directly evaluate f_{rim} of PAs in the case of the rim width n = 1 - 4, where n denotes the integration up to the nth atom in Fig. 2(b). It should be noted that the monolayer step Co atoms located at the boundary between the rim and core (Co atoms encircled by red in Fig. 2(b)) are not counted in f_{rim}. This is because such step atoms in the form of Co monolayer steps or islands on the surface of RTs do not contribute to the out-of-plane magnetization, although their coordination is lower than flat surface atoms. To find the most probable n value, we have compared $S_\perp^{rim}$ of islands (1.9 ML PA) in the cases of n = 1 - 4 with the spin magnetic moment of bilayer close packed Co clusters sandwiched between Au[19] and that of thick bcc Co films[16]. The spin magnetic moment of nanostructures is a good candidate to determine n due to its nearly independent nature of the morphology and/or substrate[1,19].

The value of f_{rim} is first evaluated from the fraction of the whole rim, which corresponds to n = 4. Note that f_{rim} was not obtained from substituting nanostructures by squares with the corresponding area, as made for the estimation of the mean lateral dimension of islands, but evaluated from the real shapes of overall observed nanostructures. Once f_{rim} for n = 4 is known, f_{rim} for n = 3, 2, and 1 can be obtained as well. The resulting f_{rim} for n = 1, 2, 3, 4 in the case of 1.9 ML PA is 12.3, 23.7, 34.1 and 43.7 %, respectively. $S_\perp^{rim}$ obtained from $S_\perp$ = 0.42 ± 0.06 μ_B/atom shown in Fig. 5(b) and f_{rim} as a function of n is shown in Fig. 7. Obviously, the values of $S_\perp/f_{rim}$ derived from n = 1 and 4 are too large and too small (3.4 ± 0.5 and 1.0 ± 0.1 μ_B/atom, respectively). It should be noted that $S_\perp^{rim}$ contains 7 $m_T^\perp$, where $m_T^\perp$ denotes the out-of-plane magnetic-dipole term[28]. The direction of $m_T^\perp$ is the same as that of the spin magnetic moment and the absolute value of 7 $m_T^\perp$ is between 0.2 and 0.3 μ_B/atom for Co clusters and thin films[19,29]. Hence, the values of $S_\perp^{rim}$ shown in Fig. 7 could be overestimated compared to the intrinsic spin magnetic moment. $S_\perp^{rim}$ for n = 3 (1.2 ± 0.2 μ_B/atom) is even smaller than the in-plane spin magnetic moment $S_\parallel$ of thick bcc Co films (1.44 μ_B/atom[16]) if the contribution of 7$m_T^\perp$ is considered. A smaller $S_\perp^{rim}$ than $S_\parallel$ of thick bcc Co films is inappropriate since the spin magnetic moment of low-coordinated atoms is enhanced due to the narrowing of the 3d band and an increase in the density of states near the Fermi level. Consequently, only n = 2 remains as a realistic number ($S_\perp^{rim}$: 1.8 ± 0.3 μ_B/atom). With n = 2, the values of f_{rim} for 3.4 and 6.0 ML PA are also evaluated as 19.2 and 5.2 %, respectively. Note that n = 2 is seen in another system showing rim-core magnetic structure[8], in good agreement with our results.

The extracted $L_\perp^{rim}$ and $S_\perp^{rim}$ at each coverage are shown by green circles in Fig. 5. We have confirmed no significant change in the magnetic moments of the rim atoms with respect to the Co coverage. This finding is reasonable since the atomic coordination, which determines the magnitude of magnetic moments[1], is independent of morphological changes at the rim. Although the contribution of $m_T^\perp$ is sensitive to the change of atomic coordination, that of the rim thus would be

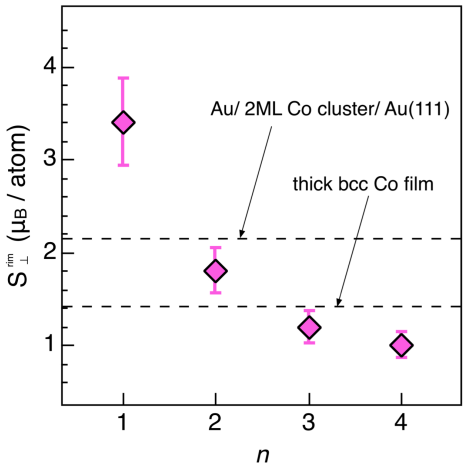

FIG. 7: (Color online) Out-of-plane spin magnetic moment of the rim atoms, $S^{rim}_{\perp}$, in bcc Co islands (1.9 ML PA) as a function of the width n of the rim atoms showing the out-of-plane magnetization. The upper and lower dashed lines represent the spin magnetic moments of bilayer close packed Co clusters sandwiched between Au (ref.19) and thick bcc Co films (ref.16). The vertical error bars derive from the standard deviations of $S^{rim}_{\perp}$.

constant against the morphological change. $S^{rim}_{\perp}$ (1.7-1.9 μ_B/atom) is larger than $S_{\parallel} = 1.3 \pm 0.1$ μ_B/atom of 3.4 ML RT in Fig. 3(a), in accordance with the reduced atomic coordination. $L^{rim}_{\perp}$ of bcc Co islands, 0.59 ± 0.08 μ_B/atom, is the highest among 2D Co nanostructures reported so far.

E. Origin of rim-core magnetic structure

Immediate questions here are (a) Why is the width of the rim atoms showing the out-of-plane magnetization limited to two ($n = 2$)? and (b) Why is the blocking temperature (T_b) of very small islands enhanced up to room temperature?

As for (a), the atomic relaxation near the rim can cause the narrow width of the out-of-plane magnetized rim. While we argue that the atomic relaxation in the whole bcc Co nanostructures is not likely in this study as discussed above, rim atoms in nanostructures are typically more sensitive to the strain than core atoms. Hence, the change of the magnetization direction from the in-plane direction favored in the core to the out-of-plane direction for several layers in the rim is probable. In such a case as the atomic relaxation is negligible also in the rim, the hybridization of Au atoms with the rim atoms would play an important role for the determination of n. At the interface, the rim and Au atoms are vertically arranged, which is not the case of RT or core atoms. In such an interface, *ab initio* calculations reveal the emergence of the out-of-plane magnetization for a transition metal system, which has the in-plane magnetization without the vertical interface[30]. Since the hybridization of rim atoms with surrounding Au atoms are effective for only a few atomic distances from the interface, $n = 2$ is a reasonable number and the coexistence of the out-of-plane magnetized rim and the in-plane magnetized core is probable. Although we cannot conclude whether the atomic relaxation or hybridization is more plausible here, it should be emphasized that both cases reveal the importance of the rim atoms to generate the out-of-plan magnetization in the bcc Co nanostructures.

As for (b), one reason derives from the vertical stacking of islands. The increased number of the rim and core atoms enhances their ferromagnetic coupling energies compared to 1 ML height islands with the same lateral size. Another hint is given by a large difference in T_b of the rim atoms in bcc Co islands embedded in Au ($\sim$ 300 K) and T_b in close packed Co nanostructures on Pt(111) ($\sim$ 100K)[8], even though both systems have n = 2 to establish their long range ferromagnetic ordering. It is experimentally[2] and theoretically[31] well known that MAEs of 3d transition metal systems increase by forming 3d-5d interface with non magnetic 5d materials. As for Co-Au system, Luis *et al.* demonstrated that the MAE of Co nanoparticles capped with Au was significantly enhanced, leading to an increase of T_b by a factor of 3 compared to the uncapped ones[32]. This is due to strong SO coupling of Au atoms, which couple to surface Co atoms via Co-Au hybridization. The rim atoms in PAs in this study are covered by Au, in contrast to vacuum in ref.8 and hence higher T_b is expected. The higher T_b is also plausible from the significant differences in the electronic band structures between bcc and close packed Co. A perturbation theory reveals that the 3d bandwidth W (exchange splitting Δ_{ex}) is inversely (directly) proportional to MAE for uniaxial systems[3] including bcc Co[18]. For bcc Co, W is approximately 1.5 eV narrower than that of close packed Co[33,34] and Δ_{ex} is the largest among 3d transition metals in accordance with the highest spin-polarization[35]. Hence, the larger MAE of Co with bcc phase than other phases is expected, resulting in higher T_b as well. Note that these two effects also enhance T_b of the core atoms, stabilizing the in-plane magnetization. As manifested above, such refinement of surrounding atoms and electronic band structures toward larger MAE in addition to the vertical stacking could establish the ferromagnetic order of the rim and core atoms in small bcc Co islands even at room temperature, leading to the coexistence of the out-of-plane and in-plane remanences.

F. Magnetic anisotropy

The importance of the specific electronic band structure of the bcc Co phase toward larger MAE can be actually seen in the formula of the MAE of the rim atoms caused by SO interaction, $\Delta E_{SO} \sim - \alpha \xi_{3d} (L^{rim}_{\parallel}$

- $L_{\perp}^{rim}$)/$(4\mu_B)^5$ where α depends on the relationship between W and Δ_{ex}[29], and $\xi_{3d} \sim 70$ meV is the SO constant for Co[19]. $L_{\parallel}^{rim}$ - $L_{\perp}^{rim}$ is experimentally derived as - 0.28 μ_B/atom for PAs[36]. Considering the room temperature out-of-plane remanence as shown in Fig. 4(b), the perpendicular MAE per bcc Co island, NΔE_{SO} (N = 200: a typical number of rim atoms in bcc Co islands), must exceed superparamagnetic limit of 645 meV (25 k_BT at 300 K)[37]. Consequently, α of 0.66 corresponding to ΔE_{SO} of 3.2 meV is at least required, which is considerably larger than α of 0.2 for close packed Co nanostructures[19,29]. This enhancement is reasonable since α is enhanced according to the relative increase of Δ_{ex} to W[29], following the differences in the electronic band structures between bcc Co phase and other phases discussed in the previous paragraph. Consequently, experimental results suggest that the MAE of rim atoms in bcc Co islands is enhanced at least by a factor of 3 compared to that in close packed Co nanostructures (0.9 meV)[8].

So far, the atomically sharp magnetic boundary between the out-of-plane magnetized rim atoms and the in-plane magnetized core atoms is assumed for simplicity. The boundary width relies on the balance between MAE and exchange energy J, i.e., larger MAE and smaller J lead to a narrower boundary width. Actually, Fe atoms in Fe thin films on W(110) with larger MAE of 4.2 meV and smaller J of 8.7 meV show the boundary width of one or two atomic sites[38]. The situation is rather similar to the Co rim atoms in this study (MAE: 3.2 meV, J: 7.5 meV[4]), suggesting also an extremely sharp magnetic boundary between the rim and core atoms in bcc Co nanostructures. The magnetic boundary width w can be evaluated as $2\sqrt{A/K_{eff}}$, where A and K_{eff} denote the exchange stiffness and the effective anisotropy constant. With K_{eff} of 3.2 meV/atom obtained from our experimental result and A of 7.0×10^{-12} J/m[39], the w in this study is indeed estimated to be ~ 0.6 nm corresponding to several atomic sites, which reveals that our assumption of the atomically sharp magnetic boundary is not unrealistic. Such a balance can be seen for other Co nanostructures[40], resulting in the noncollinear magnetic structures at the atomic scale as well.

IV. CONCLUSIONS

In conclusion, we have used XMCD to investigate magnetic properties of metastable bcc Co thin films and nanostructures on Au(001). While thin films show only the in-plane magnetization, the out-of-plane magnetization emerges additionally in nanostructures. Especially, the coexisting in-plane and out-of-plane remanences are confirmed for small islands with the typical average size of $\sim$ 4 nm. The observed out-of-plane magnetization of nanostructures shows the coverage dependence as reported in other systems. Its magnitude is, however, unexpectedly smaller than the in-plane magnetization of thin films by a factor of more than 3. Combining these XMCD results with the results of surface analysis technique by STM, a rim-core magnetic structure of nanostructures is proposed.

The validity of this rim-core magnetic structure is reinforced by the intrinsic in-plane magnetization of the core atoms revealed with XMCD-PEEM. Extracted magnetic moments of the rim atoms show larger values compared to those of thin films possibly due to (1) the reduced atomic coordination in the rim, (2) the effective interfacial effect such as the atomic relaxation or the hybridization between Co and surrounding Au atoms, and (3) the specific electronic band structure in the bcc Co phase. In accordance with the large magnetic moments, the MAE of the rim atoms results in a huge value of 3.2 meV/atom. The width of the magnetic boundary between the out-of-plane magnetized rim atoms and the in-plane magnetized core atoms is evaluated to be ~ 0.6 nm, supporting the proposed rim-core model with the atomically sharp magnetic boundary. We hope that reliable calculations will be performed in the future for further understanding of this complex magnetic structure.

V. ACKNOWLEDGEMENTS

We thank M. Kotsugi, S. Itoda, S. Komori, Y. Nakatsu and Y. Suzuki for technical assistances and scientific advices in XMCD-PEEM and Kerr measurements. We gratefully acknowledge W. Wulfhekel for fruitful discussions. A part of the research was conducted under the financial support of Grant in Aid for JSPS Fellows.

* toshio.miyamachi@kit.edu

[1] P. Gambardella, S. Rusponi, M. Veronese, S. S. Dhesi, C. Grazioli, A. Dallmeyer, I. Cabria, R. Zeller, P. H. Dederichs, K. Kern, C. Carbone, and H. Brune, Science **300**, 1130 (2003).

[2] J. Bartolomé, L. M. García, F. Bartolomé, F. Luis, R. López-Ruiz, F. Petroff, C. Deranlot, F. Wilhelm, A. Rogalev, P. Bencok, N. B. Brookes, L. Ruiz, and J. M. González-Calbet, Phys. Rev. B **77**, 184420 (2008).

[3] J. Stöhr, J. Magn. Magn. Mater. **200**, 470 (1999).

[4] P. Gambardella, A. Dallmeyer, K. Maiti, M. C. Malagoli, W. Eberhardt, K. Kern, and C. Carbone, Nature **416**, 301 (2002).

[5] P. Bruno, Phys. Rev. B **39**, R865 (1989).

[6] H. A. Dürr, S. S. Dhesi, E. Dudzik, D. Knabben, G. van der Laan, J. B. Goedkoop, and F. U. Hillebrecht, Phys. Rev. B **59**, R701 (1999).

[7] P. Ohresser, N. B. Brookes, S. Padovani, F. Scheurer, and H. Bulou, Phys. Rev. B **64**, 104429 (2001).

[8] S. Rusponi, T. Cren, N. Weiss, M. Epple, P. Buluschek, L. Claude, and H. Brune, Nature Mater. **2**, 546 (2003).

[9] S. Chikazumi, *Physics of Ferromagnetism* (Oxford Univ. Press, New York, 1997).

[10] S. Sun, C. B. Murray, D. Weller, L. Folks, and A. Moser, Science **287**, 1989 (2000).

[11] V. Skumryev, S. Stoyanov, Y. Zhang, G. Hadjipanayis, D. Givord, and J. Nogués, Nature **423**, 850 (2003).

[12] T. Kawagoe, T. Miyamachi, M. Someta, T. Kudo, and S. Suga, Surf. Sci. **602**, L15 (2008).

[13] Y. Saitoh, H. Kimura, Y. Suzuki, T. Nakatani, T. Matsushita, T. Muro, T. Miyahara, M. Fujisawa, K. Soda, S. Ueda, H. Harada, M. Kotsugi, A. Sekiyama, and S. Suga, Rev. Sci. Instrum **71**, 3254 (2000).

[14] N. Spiridis, T. Ślęzak, M. Zajac, and J. Korecki, Surf. Sci. **566**, 272 (2004).

[15] L. Z. Mezey, J. Giber, Jpn. J. Appl. Phys. **21**, 1569 (1982).

[16] P. Ryan, R. P. Winarski, D. J. Keavney, J. W. Freeland, R. A. Rosenberg, S. Park, and C. M. Falco, Phys. Rev. B **69**, 054416 (2004).

[17] Y. Z. Wu, H. F. Ding, C. Jing, D. Wu, G. L. Liu, V. Gordon, G. S. Dong, X. F. Jin, S. Zhu, and K. Sun, Phys. Rev. B **57**, 11935 (1998).

[18] X. Liu, R. L. Stamps, R. Sooryakumar, and G. A. Prinz, Phys. Rev. B **54**, 11903 (1996).

[19] T. Koide, H. Miyauchi, J. Okamoto, T. Shidara, A. Fujimori, H. Fukutani, K. Amemiya, H. Takeshita, S. Yuasa, T. Katayama, and Y. Suzuki , Phys. Rev. Lett. **87**, 257201 (2001).

[20] N. Weiss, T. Cren, M. Epple, S. Rusponi, G. Baudot, S. Rohart, A. Tejeda, V. Repain, S. Rousset, P. Ohresser, F. Scheurer, P. Bencok, and H. Brune, Phys. Rev. Lett. **95**, 157204 (2005).

[21] C. T. Chen, Y. U. Idzerda, H.-J. Lin, N. V. Smith, G. Meigs, E. Chaban, G. H. Ho, E. Pellegrin, and F. Sette, Phys. Rev. Lett. **75**, 152 (1995).

[22] B. T. Thole, P. Carra, F. Sette, and G. van der Laan, Phys. Rev. Lett. **68**, 1943 (1992).

[23] The possibility as the core atoms in PA are responsible for the $\mathbf{B}_\perp$ XMCD signal can be excluded since $L_\perp$ and $S_\perp$ of PA decrease with the increase of the coverage or the ratio of core atoms relative to rim atoms.

[24] F. E. Gabaly, S. Gallego, C. Muõz, L. Szunyogh, P. Weinberger, C. Klein, A. K. Schmid, K. F. McCarty, and J. de la Figuera, Phys. Rev. Lett. **96**, 147202 (2006).

[25] H. W. Zhao, Y. Z. Wu, C. Won, F. Toyoma, and Z. Q. Qiu, Phys. Rev. B **66**, 104402 (2002).

[26] Y. Nahas, V. Repain, C. Chacon, Y. Girard, J. Lagoute, G. Rodary, J. Klein, S. Rousset, H. Bulou, and C. Goyhenex, Phys. Rev. Lett. **103**, 067202 (2009).

[27] B. Voigtländer, G. Meyer, and N. M. Amer, Phys. Rev. B **44**, 10354 (1991).

[28] R. Wu, and A. Freeman, Phys. Rev. Lett. **73**, 1994 (1994).

[29] D. Weller, J. Stöhr, R. Nakajima, A. Carl, M. G. Samant, C. Chappert, R. Mégy, P. Beauvillain, P. Veillet, and G. A. Held , Phys. Rev. Lett. **75**, 3752 (1995).

[30] M. Tsujikawa, A. Hosokawa, and T. Oda, Phys. Rev. B **77**, 054413 (2008).

[31] Y. Xie, and J. A. Blackman, Phys. Rev. B **74**, 054401 (2006).

[32] F. Luis, J. Bartolomé, F. Bartolomé, M. J. Martínez, L. M. García, F. Petroff, C. Deranlot, F. Wilhelm, and A. Rogalev, J. Appl. Phys. **99**, 08G705 (2006).

[33] G. A. Prinz, E. Kisker, K. B. Hathaway, K. Schröder, and K. H. Walker, J. Appl. Phys. **57**, 3024 (1985).

[34] D. A. Papaconstantopoulos, *Handbook of the Band Structure of Elemental Solids* (Plenum, New York, 1986).

[35] S. Yuasa, A. Fukushima, H. Kubota, Y. Suzuki, and K. Ando, Appl. Phys. Lett. **89**, 042505 (2006).

[36] $L_\parallel^{rim}$ is evaluated from the formula $L_\parallel^{rim} f_{rim} + L_\parallel^{core}(1 - f_{rim}) = L_\parallel$. $L_\parallel$ of 0.28 ± 0.03 μ_B/atom for 3.4 ML PA is obtained from the XAS and XMCD spectra shown in Fig. 3b. The values of f_{rim} and $L_\parallel^{core}$ are obtained from STM and XMCD-PEEM measurements. Note that $L_\parallel^{rim}$, $L_\parallel^{core}$ and $L_\parallel$ of RT are comparable.

[37] O. Fruchart, M. Klaua, J. Barthel, and J. Kirschner, Phys. Rev. Lett. **83**, 2769 (1999).

[38] M. Pratzer, H. Elmers, M. Bode, O. Pietzsch, A. Kubetzka, and R. Wiesendanger Phys. Rev. Lett. **87**, 127201 (2001).

[39] F. Meier, K. von Bergmann, P. Ferriani, J. Wiebe, M. Bode, K. Hashimoto,S. Heinze, and R. Wiesendanger, Phys. Rev. B **74**, 195411 (2006).

[40] P. Gambardella, A. Dallmeyer, K. Maiti, M. C. Malagoli, S. Rusponi, P. Ohresser, W. Eberhardt, C. Carbone, and K. Kern, Phys. Rev. Lett. **93**, 077203 (2004).